# Paleoclimate Reconstructions of Tropical Sea Surface Temperatures from Precipitation Proxies: Methods, Uncertainties, and Nonstationarity

JASON C. FURTADO, EMANUELE DI LORENZO, KIM M. COBB, AND ANNALISA BRACCO

*School of Earth and Atmospheric Sciences, Georgia Institute of Technology, Atlanta, Georgia*

ABSTRACT

Proxy-based paleoclimate reconstructions of tropical sea surface temperature (SST) fields may lead to better constraints of tropical climate variability in climate model projections. In this study, the authors quantify uncertainties associated with two popular SST anomaly reconstruction methods that have been applied over the last millennium. The first reconstruction method exploits the high correlation between the leading modes of variability of global precipitation and SSTs; the second method uses a multiregression model that exploits the multiple modes of covariability between precipitation and SSTs. Regardless of the proxy network density, the first method has skill only in the tropical eastern Pacific and misses some ENSO events. By contrast, the multiregression approach demonstrates high skill throughout the tropical Indo-Pacific region and predicts all ENSO events correctly. The advantage of the multiregression method lies in the second mode of covariability between SSTs and precipitation, which explains nearly 15% of the covariability between the two variables. However, when the period 1950–2000 is considered, the authors find that the nonstationarity in the second mode of covariability between SST and precipitation leads to a significant reduction of skill in the Indian Ocean and the warm pool region. This change suggests that the underlying stationarity assumption common in most climate field reconstruction methods needs to be treated more carefully, particularly in the tropics.

## 1. Introduction

Paleoclimate reconstructions of tropical sea surface temperature (SST) fields are used to characterize the range of tropical climate variability and may improve our understanding of the role that the tropics play in global climate change. These reconstructions use a variety of proxy records ranging from tree rings and ice cores to corals and marine sediments in both the tropics and extratropics (e.g., Stahle et al. 1998; Evans et al. 2002). Although some of these proxies measure changes in tropical SSTs more directly by exploiting the relationship between temperature and a geochemical proxy (e.g., $\delta^{18}O$ in corals), most tropical proxies capture changes in precipitation (e.g., lake sediments, tree rings, speleothems, and ice cores from tropical glaciers), which are only indirectly related to SSTs. In the tropics, changes in precipitation are dynamically linked to SSTs

through the El Niño–Southern Oscillation (ENSO) phenomenon (e.g., Wyrtki 1975; Rasmusson and Carpenter 1982), which represents the leading mode of variability for both precipitation and SST (e.g., Dai and Wigley 2000). This linkage is evident from principal component analysis (PCA) (e.g., Obukhov 1947; Lorenz 1956; Kutzbach 1967) of observations and modeled data, which show that the first principal component (PC-1) time series of precipitation is strongly correlated with the Niño-3.4 index ($r > 0.9$ for all precipitation datasets), a measure of ENSO activity (Fig. 1, left). The spatial expression of the leading mode of precipitation (Fig. 1, right) exhibits strong loadings in the central tropical Pacific and warm pool regions and is reminiscent of the horseshoe pattern in SST associated with ENSO (e.g., Wallace et al. 1998).

The strong resemblance between the leading precipitation and SST modes suggests that precipitation proxy records located in major loading regions will have high skill in reconstructing past ENSO conditions. This assumption is the basis for using single paleoprecipitation reconstructions to reconstruct tropical SST variations. Single proxy reconstruction methods use an individual

*Corresponding author address:* Jason C. Furtado, School of Earth and Atmospheric Sciences, Georgia Institute of Technology, 311 Ferst Drive, Atlanta, GA 30332-0340.
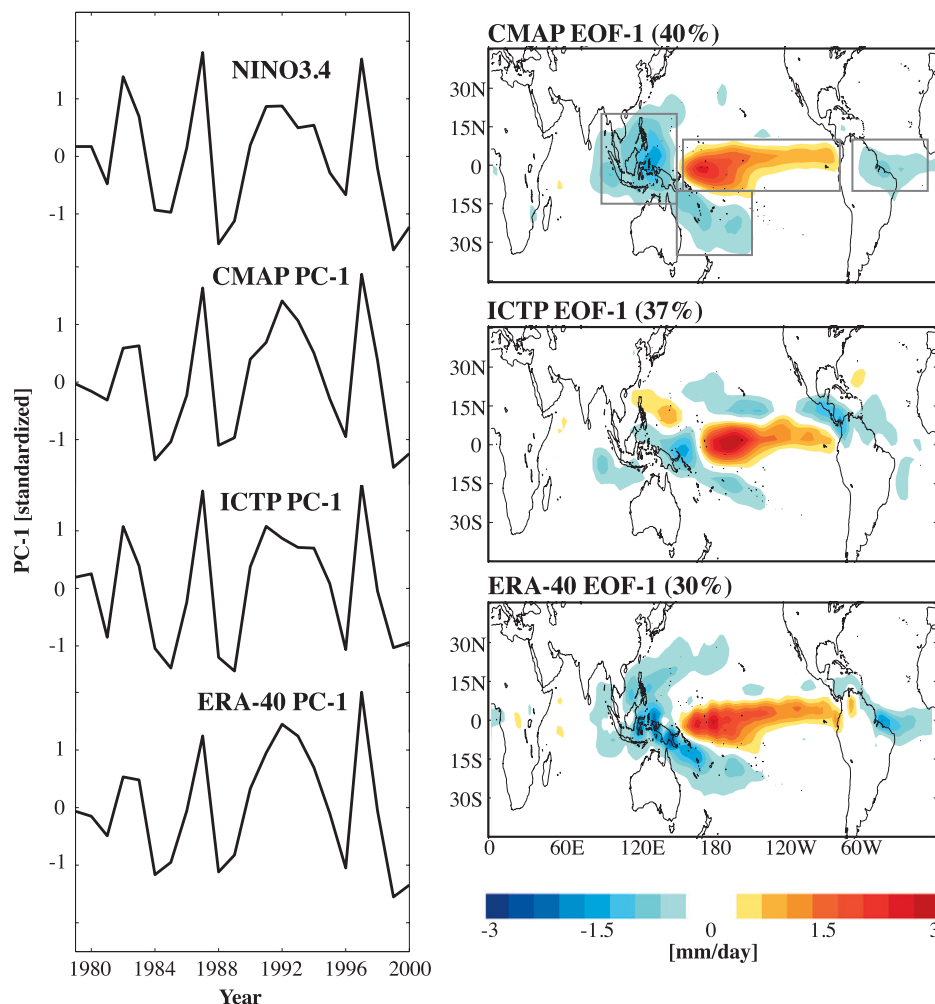E-mail: jason.furtado@eas.gatech.edu

FIG. 1. (left) Annually averaged Niño-3.4 index from 1979 to 2000 and the first principal component (PC-1) time series of annual-mean global precipitation anomalies from 1979 to 2000 for the three precipitation datasets (CMAP, ICTP model output, and ERA-40). (right) Regression of global annual-mean precipitation anomalies onto the PC-1 time series of global precipitation anomalies for the three precipitation datasets. Percent variance explained by the leading mode of precipitation variability included in the title of each plot. Gray boxes in CMAP EOF-1 are described in the text.

record from corals (e.g., Cole and Fairbanks 1990; Urban et al. 2000; Tudhope et al. 2001), marine sediments (e.g., Rein et al. 2004), tree rings (e.g., Michaelson 1989; D'Arrigo et al. 2005), lake sediments (e.g., Rodbell et al. 1999; Moy et al. 2002), ice cores (Thompson et al. 1985; Bradley et al. 2003), and speleothems (e.g., Rasbury and Aharon 2006; Partin et al. 2007) to reconstruct tropical Pacific SST variability. First, the proxy record is calibrated with SSTs or the Niño-3.4 index over a period when both proxy and instrumental data are available. If this calibration yields a significant correlation between the proxy and SST, the proxy record is then used as a surrogate of past ENSO activity and hence tropical Pacific SST anomalies. Despite the apparent strength of this method, large uncertainties in these types of re-

constructions exist because of the inability of the proxy to record a specific climate parameter perfectly (microenvironmental effects, for example), and because a local climate signal may poorly represent large-scale climate processes.

Multiproxy reconstructions reduce the uncertainties associated with single proxy reconstructions by using numerous proxies of various types (e.g., corals, tree rings, and sediments) from different locations, under the assumption that their shared signals represent large-scale climate patterns. Typically, such reconstructions create a climate pattern template by calibrating each proxy record against the instrumental record and use these templates to extrapolate back in time. Examples of methods that use these climate pattern templates are

1) PCA (e.g., Mann et al. 1998) and 2) reduced space objective analysis (e.g., Evans et al. 2002). Both methods reside in the climate field reconstruction (CFR) family (Mann et al. 2005), a group of methods favored for studying low-frequency climate variability.

Although the multiproxy approach is useful in reducing and quantifying the uncertainties of reconstruction of SST fields based on single proxies, there are several sources of error that require careful consideration. One issue is that some proxies are better able to capture tropical SST variations over others. Second, different proxies may measure different climate variables (e.g., precipitation versus temperature), making extracting a common climate signal from the multiple proxies difficult. Finally, the inherent assumption of stationarity of the climate statistics that underlies CFR methods may not always be valid (i.e., climate patterns and teleconnections may change with time) and hence the reconstructive skill may be substantially reduced. One example of nonstationary statistics in the tropics is evident in the evolution of ENSO events following the 1976–77 climate shift (e.g., Neelin 1991; Neelin et al. 1994; Trenberth and Hurrell 1994; Zhang et al. 1997; Federov and Philander 2000, 2001; Guilyardi 2006). To what extent this change in ENSO behavior impacts the overall skill of a tropical SST reconstruction has not been explicitly addressed.

The goal of this study is to quantify the uncertainties in SST reconstructions obtained using multiproxy records of precipitation by applying both empirical orthogonal function (EOF)-based and multiregression techniques to pseudoproxy data over the period 1979–2000. The EOF method yields significant skill only in the eastern tropical Pacific, where it captures most of the ENSO events, although some events have the wrong sign. Alternatively, the multiregression approach has higher skill that extends throughout the tropical Pacific and Indian Oceans and correctly predicts all ENSO events. We also show that the skill of the multiregression method is degraded when applied to the 1950–2000 interval owing to nonstationarity in the SST–precipitation relationship.

Section 2 describes the data and analysis tools used. Section 3 assesses the sensitivity of the SST reconstructions to the method and the precipitation dataset used to build the climate pattern template. Section 4 addresses the issue of nonstationarity in ENSO statistics over the last 50 years and its impact on the reconstructive skill. Section 5 explores the performance of a realistic paleoprecipitation proxy network, including how the errors in paleoprecipitation records propagate into the resulting SST reconstructions. Conclusions and suggestions for future work are presented in section 6.

## 2. Data and methods

### a. Precipitation and SST datasets

Precipitation data used in this study originate from three sources. The Climate Prediction Center Merged Analysis of Precipitation (CMAP) dataset, which combines in situ rain gauge measurements and satellite-derived estimates of precipitation (Xie and Arkin 1997), is one of two observational datasets used. The CMAP data are on a 2.5° × 2.5° horizontal grid globally and extend back to 1979. For this study, we use the "non-enhanced" version of the CMAP dataset (i.e., no assimilated data from numerical model output), though results are similar if the enhanced product is used (not shown). A second observational precipitation dataset used in this study is the 40-yr European Centre for Medium-Range Weather Forecasts Re-Analysis (ERA-40) (e.g., Simmons and Gibson 2000). These data are interpolated onto a 2.5° by 2.5° horizontal grid globally, and the dataset extends from 1957 to 2002.

In addition, we use precipitation output from a control run of the International Center for Theoretical Physics (ICTP) atmospheric general circulation model (AGCM) using eight vertical layers and T30 horizontal resolution (3.75° × 3.75° on a longitude–latitude grid). The physical parameterizations of the model are described in Molteni (2003), and prior applications of this configuration can be found in Bracco et al. (2006) and Kucharski et al. (2006, 2007). The model is forced using prescribed monthly mean SST anomalies from the National Oceanic and Atmospheric Administration Extended Reconstructed SSTs dataset (NOAA ER SSTs) (Smith and Reynolds 2003). The model run extends from 1950 to 2000.

To evaluate the reconstruction methods, we restrict the data to only 1979–2000, the common period for all datasets. All fields are annually averaged (January–December) and detrended. Annual-mean anomalies are derived by removing the 1979–2000 mean from the annual means of each year. When evaluating the effect of nonstationary climate statistics on the skill of the reconstructions, the climate pattern template is constructed using detrended annual-mean precipitation anomalies for each year from the full 51-yr model control run along with the corresponding detrended annual-mean SST anomalies from the NOAA ER SSTs. Sea surface temperature and precipitation data are spatially smoothed using a 5-point averaging scheme—the value assigned to each grid point is the average of the values in that grid point and the four adjacent grid points to the north, south, east, and west. This smoothing technique reduces the effects of mesoscale features in the two fields while still retaining the large-scale features that are of

interest in this study. SST anomaly reconstructions are performed only from 30°S to 30°N (referred to as *the tropics* in this paper) and are compared to the NOAA ER SSTs to assess errors in the reconstructions.

### b. Precipitation proxy network

One objective of our study is to assess how well a given proxy network of paleoprecipitation data can reconstruct tropical Indo-Pacific SST anomalies. Figure 2a illustrates the paleoprecipitation proxy network employed in this study (black dots), with the names and types of proxies listed in Table 1. The proxy network consists of both terrestrial and oceanic proxies scattered throughout the tropics. Several of the proxies lie in areas of high precipitation variance (shaded contours in Fig. 2a; e.g., those in the tropical Pacific Ocean) while others do not (e.g., those in the far western Indian Ocean, Africa, and off of the Australian coast). We create a pseudoproxy network based on our realistic proxy network by replacing each proxy record with CMAP data from that proxy's location. Because multiple sites reside within certain grid boxes, only 39 of the 45 locales in Table 1 represent unique grid points for the reconstruction.

### c. Reconstruction methods

#### 1) EOF METHOD

The EOF method exploits the close relationship between SSTs and precipitation in the tropics, dominated by coupled ENSO dynamics, to reconstruct SSTs from precipitation. Here, we only use the first EOF (EOF-1) of precipitation and SSTs because the PC-1 time series of global precipitation variability explains nearly 80% of the variability in global SST variability (see Fig. 1).

Letting $\mathbf{V}_{SST}$ and $\mathbf{U}_{SST}$ represent EOF-1 of global SSTs and its associated PC time series, respectively, SST anomalies ($\mathbf{y}_{SST}$; i.e., the unknown) can be approximated as

$$\mathbf{y}_{SST} \approx \mathbf{V}_{SST}\mathbf{U}_{SST}. \qquad (1)$$

Similarly, for precipitation anomalies ($\mathbf{x}_p$),

$$\mathbf{x}_p \approx \mathbf{V}_p\mathbf{U}_p, \qquad (2)$$

where $\mathbf{V}_p$ is EOF-1 of global precipitation anomalies and $\mathbf{U}_p$ is the corresponding PC time series. Both $\mathbf{V}_{SST}$ and $\mathbf{V}_p$ are assumed to be time invariant implying that SST and precipitation have stationary statistics. Given $\mathbf{x}_p$ and $\mathbf{V}_p$, we can estimate the PC time series using a least square approach:

$$\hat{\mathbf{U}}_p = (\mathbf{V}_p^T\mathbf{V}_p)^{-1}\mathbf{V}_p^T\mathbf{x}_p, \qquad (3)$$

where the caret denotes an estimate.

As noted before, $\mathbf{U}_p$ and $\mathbf{U}_{SST}$ are significantly correlated so that $\mathbf{U}_{SST} = \alpha\hat{\mathbf{U}}_p$, where the correction factor ($\alpha$) is chosen as the regression coefficient between the PC-1 time series of SST and the PC-1 time series of the precipitation data from 1979 to 2000. Replacing $\mathbf{y}_{SST}$ with $\hat{\mathbf{y}}_{SST}$ and setting $\mathbf{U}_{SST} = \alpha\hat{\mathbf{U}}_p$, (1) becomes

$$\hat{\mathbf{y}}_{SST} = \alpha\mathbf{V}_{SST}\hat{\mathbf{U}}_p, \qquad (4)$$

which allows us to reconstruct tropical SST anomalies using the known leading modes of variability of global SSTs and precipitation anomalies. Note that this method only works for the PC-1 time series of SST because of its high correlation with the PC-1 time series of precipitation. Higher modes of precipitation and SST are not correlated, and thus this method would not be adequate unless one computes explicitly the leading modes of covariability between SST and precipitation. This is the basis for the multiregression approach illustrated below.

#### 2) MULTIREGRESSION METHOD

The other reconstruction method used in this study is based on multiregression or covariance modeling, a technique that uses least squares fitting to estimate one variable from another (e.g., Wunsch 2006). This approach can be viewed as an extension of the EOF method in that it accounts for more modes of covariability between SSTs and precipitation, rather than the variability of each climate variable separately.

Considering two variables, the predictand $\mathbf{y}$ (SSTs) and the predictor $\mathbf{x}$ (precipitation), the linear relationship between these two variables can be written mathematically as

$$\mathbf{y} = \mathbf{E}\mathbf{x} + \mathbf{n}, \qquad (5)$$

where $\mathbf{E}$ is a mapping matrix from $\mathbf{x}$ onto $\mathbf{y}$, and $\mathbf{n}$ is the error associated with linearization. If no known analytical relationship exists between $\mathbf{x}$ and $\mathbf{y}$, a statistical relationship can be used for $\mathbf{E}$. The optimal statistical choice for $\mathbf{E}$ is one that minimizes the mean square error (MSE), (i.e., $\langle\mathbf{n}\mathbf{n}^T\rangle$, where angle brackets denote the averaging operator) between $\mathbf{y}$ and $\hat{\mathbf{y}}$, the estimate of $\mathbf{y}$. From (5),

$$\langle\mathbf{n}\mathbf{n}^T\rangle = \langle(\mathbf{y} - \mathbf{E}\mathbf{x})(\mathbf{y} - \mathbf{E}\mathbf{x})^T\rangle$$
$$= \langle\mathbf{y}\mathbf{y}^T\rangle + \mathbf{E}\langle\mathbf{x}\mathbf{x}^T\rangle\mathbf{E}^T - 2\langle\mathbf{y}\mathbf{x}^T\rangle\mathbf{E}^T. \qquad (6)$$

By minimizing $\langle\mathbf{n}\mathbf{n}^T\rangle$, the optimal linear estimator is found to be

$$\mathbf{E} = \langle\mathbf{y}\mathbf{x}^T\rangle\langle\mathbf{x}\mathbf{x}^T\rangle^{-1} = \mathbf{C}_{yx}\mathbf{C}_{xx}^{-1}, \qquad (7)$$

### (a) Standard Deviation of CMAP Anomalies



### (b) Standard Deviation of NOAA ER SST Anomalies
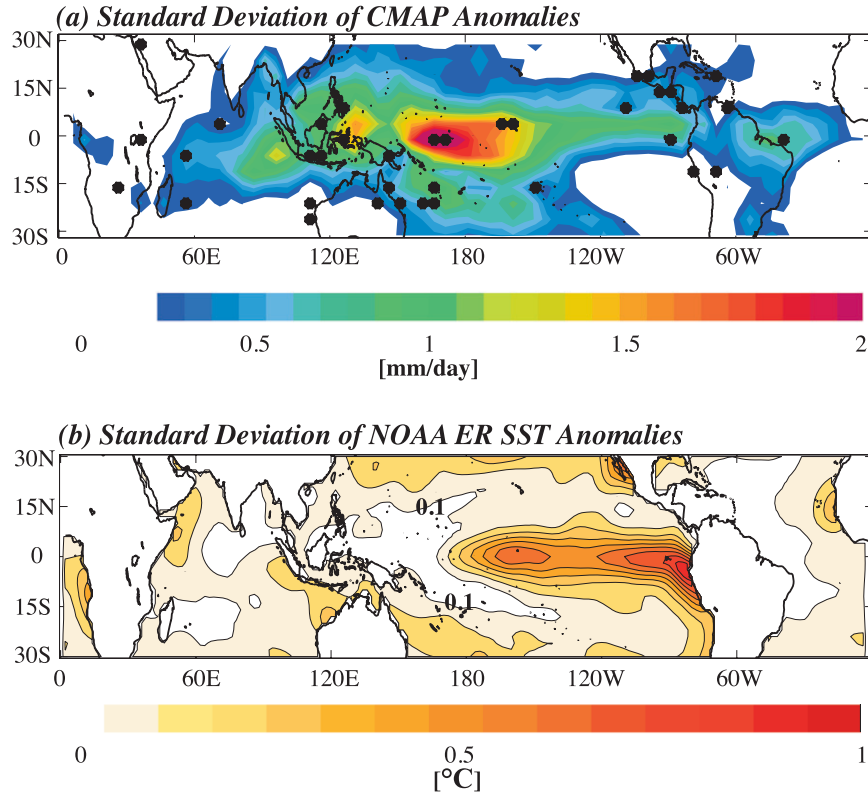


FIG. 2. (a) Standard deviation of annual-mean precipitation anomalies (mm day$^{-1}$) from CMAP (shaded color contours) from 1979 to 2000 superimposed on the proxy network locations from Table 1 (black dots). Values smaller than 0.2 mm day$^{-1}$ are not shaded. (b) Standard deviation of annual-mean SST anomalies (°C) from 1979 to 2000. Contour interval every 0.1°C; the 0.1°C contour is labeled for reference.

where $\mathbf{C}_{ij}$ is the covariance matrix between $i$ and $j$. Hence,

$$\hat{\mathbf{y}} = \mathbf{C}_{yx}\mathbf{C}_{xx}^{-1}\mathbf{x} \qquad (8)$$

is the best estimate for tropical SSTs using precipitation data provided in $\mathbf{x}$. The MSE associated with using (7) is then

$$\langle \mathbf{n}\mathbf{n}^{T}\rangle = \mathbf{C}_{yy}[1 - \mathbf{C}_{yy}^{-1}\mathbf{C}_{yx}\mathbf{C}_{xx}^{-1}\mathbf{C}_{yx}^{T}], \qquad (9)$$

which serves as an estimate of the error in our reconstructed SST anomalies.

Inverting covariance matrices with data from very large or high-resolution grids is computationally expensive. So, we degrade the spatial resolution of the precipitation and SST datasets to every other grid point within the tropics prior to covariance analysis. Before computing $\mathbf{E}$, the covariance matrices are calculated and decomposed into eigenvalues and eigenvectors. For $\mathbf{C}_{xx}$ and $\mathbf{C}_{yy}$ ($\mathbf{C}_{yx}$), we retain only those modes that explain more than 1% (5%) of the total covariance. This

additional step is performed to eliminate statistically insignificant higher-order modes of covariability. The resulting reconstructions have fewer degrees of freedom and retain larger-scale features. We also use a simple cross-validation scheme to test for robustness of the covariance statistics that enters $\mathbf{E}$. This is done by calculating $\mathbf{E}$ using a subset of the data from 11 of the 22 available years and assessing the reconstructive skill over the entire period of the data. The process is repeated 20 times with different 11-yr sets of data. We then take the average error of the 20 reconstructions and verify that it is equivalent to the one estimated by (9).

#### d. Assessing errors in the SST reconstructions

Errors in the SST reconstructions are assessed in three ways:

(1)  The root-mean-square error (RMSE):

$$\text{RMSE} = \sqrt{\text{var}(\hat{y} - y)}, \qquad (10)$$

where var($\cdots$) is the variance function normalized by $1/(N - 1)$ ($N$ is the number of samples), $\hat{y}$ is the

TABLE 1. The precipitation proxy network used in this study. Dates are given in years AD or in years before present (YBP).

| Type of proxy | Location (lat, lon) | Time period | Reference |
|---|---|---|---|
| Tree rings | El Vado (16.4°N, 96.5°W) | 1750–1990 | Therrell et al. (2002) |
| | Mzola Forest (18.2°S, 27.4°E) | 1796–1997 | Stahle et al. (1999) |
| | Nevado de Colima (19.4°N, 103.4°W) | 1553–1997 | Biondi (2001) |
| | Villareal (19.3°N, 97.5°W) | 1710–1998 | Therrell et al. (2002) |
| | Baobab Holes (18.4°S, 26.4°E) | 1846–1994 | Stahle, Gabor, Haynes, Klimowicz, and Ngwenya (unpublished data)* |
| | Bigin (7.2°S, 111.5°E) | 1839–1995 | D'Arrigo et al. (1994) |
| | Sikumi (18.3°S, 26.6°E) | 1870–1996 | Stahle et al. (1999) |
| Corals | Aqaba 18 (29.5°N, 35°E) | 1788–1992 | Heiss (1994) |
| | Cebu (10°N, 124°E) | 1859–1979 | Patzöld (1984) |
| | Secas Island (7.6°N, 82.3°W) | 1708–1984 | Linsley et al. (1994) |
| | Kiritimati (2.0°N, 157.3°W) | 1938–93 | Evans et al. (1999) |
| | Tarawa Atoll (1.0°N, 172.0°E) | 1894–1989 | Cole and Fairbanks (1990) |
| | Urvina Bay (0.4°S, 91.2°W) | 1607–1953 | Dunbar et al. (1994) |
| | Punta Pitt (0.7°S, 89.1°W) | 1936–83 | Shen et al. (1992) |
| | Mahe, Seychelles (4.6°S, 55.8°E) | 1846–1995 | Charles et al. (1997) |
| | Espiritu Santo (15°S, 167°E) | 1806–1979 | Quinn et al. (1996) |
| | New Caledonia (20.7°S, 166.2°E) | 1657–1992 | Quinn et al. (1998) |
| | Abraham Reef (22.1°S, 153.0°E) | 1635–1957 | Druffel and Griffin (1993) |
| | Amedee Lighthouse (22.3°S, 166.3°E) | 1657–1992 | Quinn et al. (1998) |
| | Bunaken (1.3°N, 124.5°E) | 1860–1990 | Charles et al. (2003) |
| | Brook Island (18.1°S, 146.2°E) | 1565–1985 | Hendy et al. (2002) |
| | Clipperton Atoll (10.3°N, 109.2°W) | 1893–1994 | Linsley et al. (2000b) |
| | Houtman Abrolhos Islands (28.3°S, 113.5°E) | 1795–1994 | Kuhnert et al. (1999) |
| | Ifaty Reef (23.9°S, 43.3°E) | 1659–1995 | Zinke et al. (2004) |
| | La Parguera (17.6°N, 64.0°W) | 1700–1989 | Winter et al. (2000) |
| | Laing Island (4.1°S, 144.5°E) | 1884–1993 | Tudhope et al. (2001) |
| | Lombok Strait (8.2°S, 115.3°E) | 1782–1990 | Charles et al. (2003) |
| | Madang (5.2°S, 145.9°E) | 1880–1993 | Tudhope et al. (2001) |
| | Maiana (1.0°N, 173.0°E) | 1840–1995 | Urban et al. (2000) |
| | Malindi (3.0°S, 40.0°E) | 1801–1994 | Cole et al. (2000) |
| | Moorea Lagoon (17.3°S, 149.5°W) | 1852–1990 | Boiseau et al. (1999) |
| | Nauru (0.5°S, 167.0°E) | 1897–1995 | Guilderson and Schrag (1999) |
| | Ningaloo Reef (21.5°S, 113.6°E) | 1878–1994 | Kuhnert et al. (2000) |
| | Palmyra Island (5.5°N, 162.8°W) | 1886–1998 | Cobb et al. (2001) |
| | Rarotonga Island (21.1°S, 159.5°W) | 1726–1997 | Linsley et al. (2000a) |
| | Saint Gilles (21°S, 55°E) | 1830–1995 | Pfeiffer et al. (2004) |
| Lake sediments | Lake Peten-Itza (16.6°N, 89.5°W) | 9000 YBP–present | Curtis et al. (1998) |
| | Lake Valencia (10°N, 66°W) | 20 000 YBP–present | Street-Perrott et al. (1989) |
| Speleothem | Borneo (4°N, 115°E) | 2000 YBP–present | Partin et al. (2007) |
| Marine sediments | Cariaco Basin (10°N, 65°W) | 19 000 YBP–present | Haug et al. (2001) |
| | Peru Lithics (12.0°S, 77.4°W) | ~12 000 YBP–present | Rein et al. (2004) |
| | Mindanao Strait (7°N, 127°E) | ~15 000 YBP–present | Stott et al. (2004) |
| Ice cores | Kilimanjaro (3°N, 37°E) | 1800–2000 | Thompson et al. (2002) |
| | Huascaràn (9°S, 77°W) | 19 000 YBP–present | Thompson et al. (1995) |
| | Quelccaya (13.5°S, 70.5°W) | 470–1980 | Thompson et al. (1985) |

* Data archived at the World Data Center for Paleoclimatology, Boulder, Colorado.

time series of reconstructed SSTs at a given point, and $y$ is the time series of observed SSTs from NOAA ER SSTs at the same point. This measure allows us to determine spatially where the reconstructions perform the best.

(2) The spatial correlation between the reconstructed and the observed SST anomalies. This measure

allows us to assess the skill of the SST reconstructions for each year. For example, strong ENSO years may reflect higher spatial correlations than non-ENSO years. Statistically significant correlations at the 95% level are found by using a Monte Carlo–like approach whereby spatial correlations are calculated between one year of observed

annual-mean SST anomalies in the tropics from 1950 to 2000 and every other year in the 1950–2000 period. A normalized probability distribution function of the correlations is then used to determine the 95% significance level (found to be $r = 0.64$). Only positive correlations are considered in significance testing since negative correlations mean that large-scale reconstructed SST patterns are of opposite sign from the observations and are hence not meaningful for our study.

(3) The reconstructive skill:

$$\text{skill} = 1 - \frac{\text{RMSE}}{\sqrt{\text{var}(y)}}. \qquad (11)$$

The measure determines how well the reconstructed anomalies compare to the observed fluctuation of SSTs. Because the standard deviation of SSTs varies across the tropics, the skill will have strong spatial dependence. Figure 2b illustrates the standard deviation of SSTs over the tropics from 1979 to 2000. The variations in SSTs are strongest in the upwelling zones of the equator and the Pacific coast of South America, where standard deviations approach $1°C$ off of the Peruvian coast. Lower variance characterizes the west Pacific warm pool and portions of the Indian Ocean. Therefore, based on (11), high skill (values near unity) arises in areas where the rms error is much smaller than the standard deviation of SSTs and vice versa.

For reconstructions using the multiregression method, the skill can be computed analytically as

$$\text{estimated skill} = 1 - \sqrt{\frac{\text{diag}(\langle \mathbf{nn}^\mathrm{T} \rangle)}{\text{var}(y)}}, \qquad (12)$$

where $\text{diag}(\langle \mathbf{nn}^\mathrm{T} \rangle)$ refers to the diagonal elements of (9). We also use (12) as an estimate for the EOF method, but $\langle \mathbf{nn}^\mathrm{T} \rangle$ contains only errors from the first covariability mode. In this way, we are able to evaluate the utility of using only the leading modes of variability in both methods.

## 3. Evaluation of reconstruction methods: 1979–2000 statistics

### a. Reconstructing SST anomalies from precipitation data using EOF-1

To examine the "best case" scenario for the EOF method, area-averaged precipitation from the four large

centers of action in EOF-1 of precipitation are used (as delimited in Fig. 1, right, gray boxes). Since these regions represent where the highest ENSO-related variance in precipitation exists, SST anomalies should be closely tied to precipitation in those regions. These regions are 1) the equatorial Pacific Ocean ($10°S–10°N$, $155°E–80°W$), 2) the Maritime Continent ($20°S–20°N$, $90°–150°E$), 3) the southwest Pacific Ocean ($35°–10°S$, $150°E–150°W$), and 4) the Nordeste region in Brazil and the adjacent tropical Atlantic Ocean ($10°S–10°N$, $70°–10°W$). This averaging would be analogous to "stacking" multiple paleoprecipitation records from the same region together.

Figure 3 shows the rms error between the reconstructed SST anomalies using the EOF method and observations (Fig. 3, left column), along with the reconstructive (Fig. 3, middle column) and estimated (Fig. 3, right column) skills, as a function of the precipitation dataset used. In all datasets, rms errors are a maximum in the central tropical Pacific, just east of the major loading center depicted in Fig. 1 (right). For the model and ERA-40, a secondary maximum in rms error exists along the South American coast. The reconstructive skill for all datasets is highest only in the eastern tropical Pacific, with the atmospheric model performing worst in terms of absolute skill and CMAP the best (Fig. 3, middle column). Elsewhere in the Indo-Pacific basin, little if any skill exists.

The estimated skill of the EOF method (Fig. 3, right column) is derived by using only the first mode of covariability between SSTs and precipitation, which strongly resembles the individual leading modes of each variable (see Fig. 6), in the multiregression method. Though not explicitly representative of the EOF method per se, this plot shows that using only the leading modes of variability of precipitation and SST restricts skill to the eastern and central Pacific. Note that the estimated skill plots predict maximum skill in the central tropical Pacific, while the EOF method has its highest skill in the far eastern tropical Pacific Ocean.

The spatial correlation coefficients between the reconstructed and observed SST anomalies (Fig. 5, black curves) have high temporal variability, with occasional negative coefficients; negative values indicate the SST reconstructions for those years capture the wrong sign of large-scale SST anomalies in the tropics. These erroneous reconstructions occur mainly during neutral or weak ENSO years (i.e., when values of Niño-3.4 are small). Half (11) of the 22 years have reconstructions with spatial correlations that exceed the 95% significance level. However, the mean spatial correlation coefficient for any dataset over all 22 years falls well below the 95% significance level.
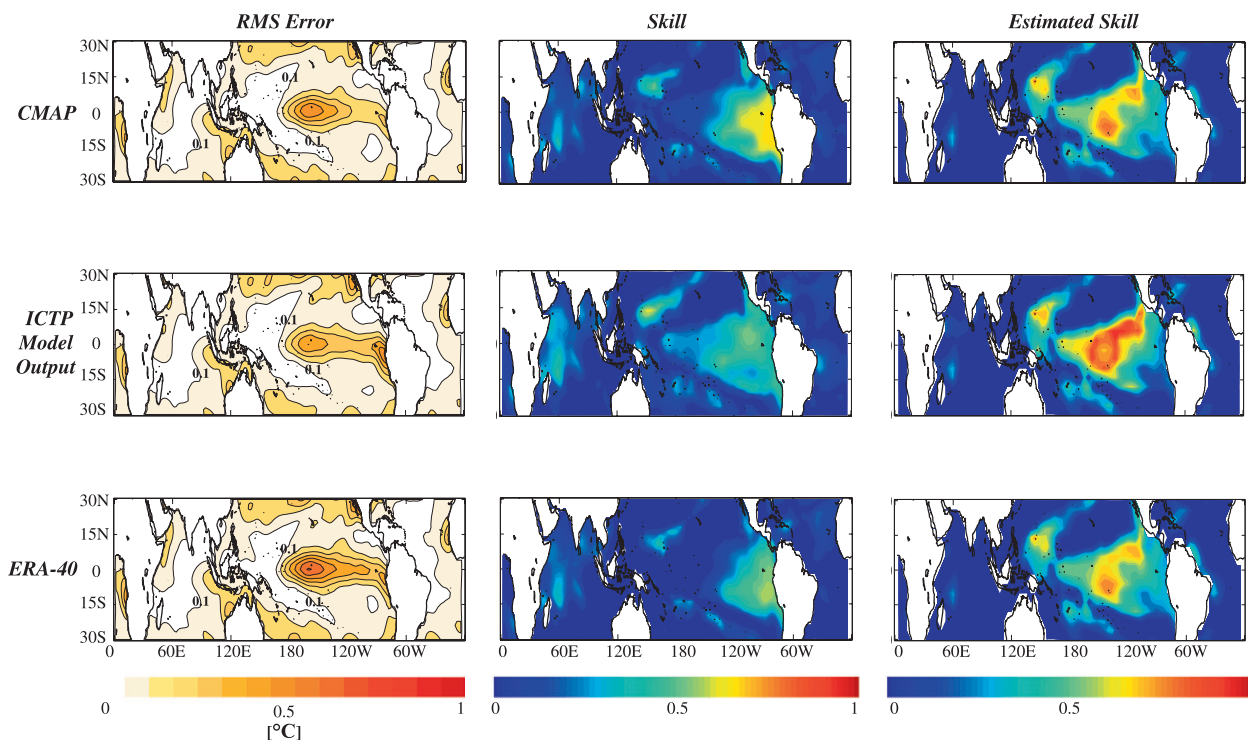
FIG. 3. Evaluation of the EOF-based reconstruction method using precipitation from CMAP, ICTP model output, and ERA-40. (left column) rms error (°C). Contour interval 0.1°C; the 0.1°C contour is labeled for reference. (middle column) Reconstructive skill (dimensionless). (right column) Estimated reconstructive skill (dimensionless), evaluated using only the first covariance mode in the multiregression model (see text for details).

## b. Reconstructing SST anomalies from precipitation data using the multiregression model

The rms error, mean skill, and estimated skill fields for the multiregression method are shown in Fig. 4. Rms errors (Fig. 4, left column) are substantially lower than those associated with the EOF method throughout the tropical oceans, with about a 70% reduction in rms error in the Pacific cold tongue region. The reconstructive skill (Fig. 4, middle column) is high over a broad area of the central and eastern tropical Pacific Ocean for all datasets. Moreover, moderate reconstructive skill now exists over the equatorial and northern Indian Ocean regions, compared to little skill with the EOF method. Quantitatively, the improvement in skill of the multi-regression method over the EOF method is roughly 30% in the eastern tropical Pacific Ocean (more so for the atmospheric model) and upward of 200% in the central tropical Pacific Ocean and the Indian Ocean. Finally, the mean skill levels match those predicted by the estimated skill maps (Fig. 4, left column), though the estimated skill fields for both observational sets (CMAP and ERA-40) highly underestimate the demonstrated skill of the multiregression model in the Indian Ocean.

When examining the spatial correlation between the reconstructed and observed SST anomalies for the multiregression method (Fig. 5, gray curves), we once again see vast improvements over the EOF method. The mean correlations range from 0.73 to 0.75, all of which are statistically significant and higher than their counterparts for the EOF method. Moreover, recon-structions for every year exhibit positive correlation coefficients, demonstrating that the multiregression model always captures the correct sign of large-scale tropical ocean features (i.e., ENSO events). Minima in the correlation coefficients coincide with neutral or weak ENSO years, as observed with the EOF method, though the variance of the correlation coefficients is less than that observed for the EOF method.

Results for the multiregression model also hold for several variants on the analysis (figures not shown). One analysis uses boreal summer and boreal winter seasonal mean precipitation and SST fields rather than annual-mean fields. Error measures for this variant were highly similar, particularly for the boreal summer SST recon-structions presumably because of the strong coupling between tropical SSTs and the Northern Hemisphere intertropical convergence zone. Two additional variants
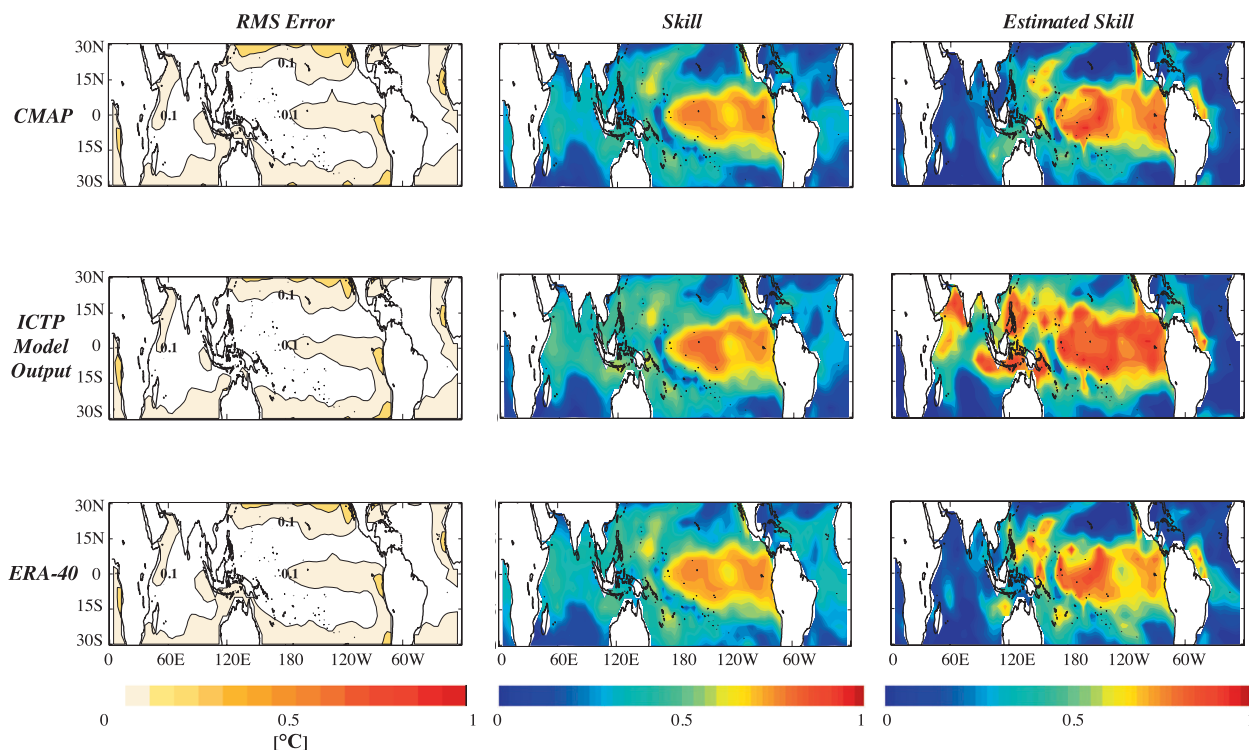
FIG. 4. Evaluation of the multiregression method using precipitation from CMAP, ICTP model output, and ERA-40. (left column) rms error (°C). Contour interval 0.1°C; the 0.1°C contour is labeled for reference. (middle column) Reconstructive skill (dimensionless). (right column) Estimated reconstructive skill of the multiregression model (dimensionless).

of the analysis included using annual-mean anomalies of precipitation and SSTs over the so-called ENSO year (i.e., June–May) instead of calendar year and also comparing our SST anomaly reconstructions with SST anomalies from the Hadley Centre SST (HadISST) dataset (Rayner et al. 2003) instead of the NOAA ER SSTs. For both of these variations, the results obtained and conclusions drawn were virtually identical those presented in this paper. These sensitivity analyses support the robustness of our results and also the robustness of the observed covariability modes with another SST dataset.

### c. Examination of modes of covariability between tropical SSTs and precipitation

As a way of examining why the multiregression method outperforms the EOF method, we conduct singular value decomposition (SVD) (Bretherton et al. 1992) analysis on the covariance matrix of tropical SSTs and tropical precipitation anomalies from 1979 to 2000 for each precipitation data source. For this SVD analysis, left singular vectors (LSVs) represent covariability between the two variables in the SST spatial domain, and right singular vectors (RSVs) represent the covariability in the precipitation spatial domain. The presentation of

each mode is as follows: 1) We calculate the expansion coefficient time series for each mode by projecting annual-mean anomaly maps of the variable onto its representative singular vectors (e.g., annual-mean SST anomaly maps are projected onto the leading mode of covariability in the SST domain: LSV-1). 2) The expansion coefficient time series are then standardized and regressed onto annual-mean anomaly fields of their respective variable. In this way, the spatial patterns of variability have meaningful units of the field itself (i.e., °C for SSTs, mm day$^{-1}$ for precipitation). Note that the regressions performed here are homogeneous, but heterogeneous regression (e.g., regressing the expansion coefficient time series for SSTs onto precipitation anomaly maps) yields virtually the same results.

Figure 6 displays the regression of tropical SST and precipitation anomalies onto the first two expansion coefficient time series from the SVD analysis (labeled mode 1 and mode 2 in the figure). For discussion, we will refer to these patterns simply as LSV-1/RSV-1 and LSV-2/RSV-2. The two leading modes of covariability together explain about 95% of the covariance between tropical precipitation and SST anomalies. LSV-1 displays the canonical ENSO signature, while RSV-1 is indistinguishable from EOF-1 of global precipitation
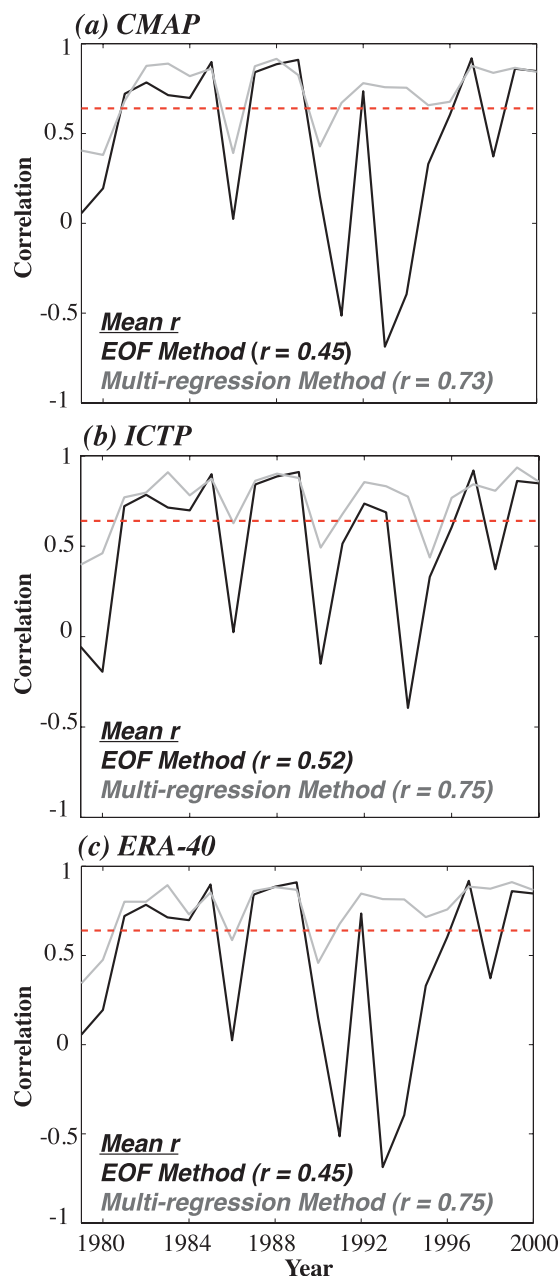
FIG. 5. Spatial correlation between the observed and reconstructed tropical SST anomalies (30°N to 30°S) from the EOF method (black curves) and the multiregression method (gray curves): Results for (a) CMAP, (b) the ICTP run, and (c) ERA-40. Mean correlation for each method also given in each figure. Red dashed line denotes the 95% significance level ($r = 0.64$).

anomalies (Fig. 1, right). Of more interest, however, is the second mode of covariability, which explains ~15% of the covariance regardless of the precipitation data used. LSV-2 displays a zonal tripole with alternating positive–negative–positive SST anomalies across the

equatorial Pacific. This SST pattern also coincides a similar zonal tripole in precipitation anomalies, as depicted by RSV-2 (Fig. 6). Note that even the model captures these patterns, albeit of slightly different spatial scale from the observational datasets. This alternating pattern of SST/precipitation anomalies across the tropical Pacific is very similar to that observed during the 1997–98 ENSO event, for example (e.g., Bell et al. 1999, their Figs. 24 and 26). This correspondence may suggest that the patterns reflect the precipitation response to eastward propagation of SST anomalies characteristic of the ''T-mode''/delayed oscillator mode of ENSO, prevalent after 1980, as opposed to the westward propagation of SSTs observed during the ''S-mode'' of ENSO prior to 1980 (Federov and Philander 2001, 2003).

The eigenvalue spectrum in Fig. 6 further illustrates the importance of including the second mode of covariability in tropical SST reconstructions. Both the first and second covariability modes are statistically significant per the North et al. (1982) criterion, with modes 3 and higher insignificantly different from each other in terms of percent variance explained.

## 4. Nonstationarity and its impacts on reconstructive skill

The assessments of tropical SST reconstructions presented thus far have been based solely using statistics from the 1979–2000 period. This period of time is relatively short and therefore affects the significance of our results through potential bias, especially considering that the two largest positive ENSO events in recorded observational history occurred during that period (i.e., 1982–83 and 1997–98). Furthermore, observed changes in the character of Pacific variability after the 1976–77 climate shift (e.g., Trenberth and Hurrell 1994; Zhang et al. 1997) also introduce a source of bias to the 1979–2000 climate statistics. Increasing the length of our tropical precipitation and SST time series allows us to address the potential influence of nonstationarity in the joint statistics between the two variables. For this analysis, we rely on the 51-yr ICTP AGCM control run. Results from section 3 suggest that use of the model precipitation fields is reliable for assessing longer-term statistics because of the close match between the results from the model and those from observations.

Before proceeding with the 1950–2000-based reconstructions, we examine the difference in the patterns of covariability of the ICTP AGCM precipitation and NOAA ER SSTs from 1979 to 2000 (Fig. 6) with those from 1950 to 1978 and 1950 to 2000 (Fig. 7). The major differences between the two periods arise in LSV-2. From 1950 to 2000, the Indian Ocean and eastern Pacific
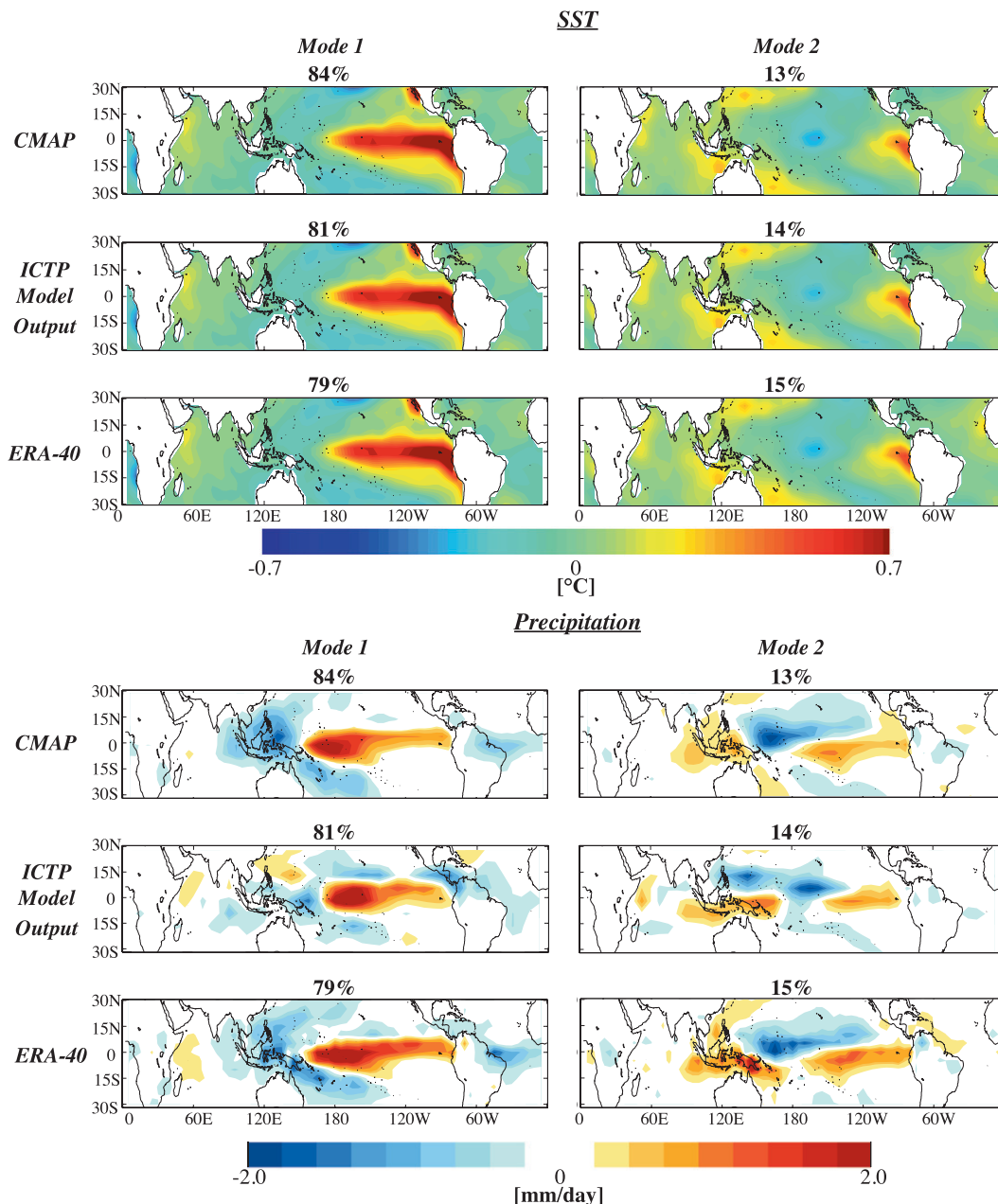
FIG. 6. The two leading modes of covariance between tropical SST and precipitation anomalies (30°S–30°N) from 1979 to 2000 for each dataset: (top) Regression of annual-mean SST anomalies (°C) onto the first and second expansion coefficient time series of the left singular vectors of the SVD analysis; (bottom) regression of annual-mean precipitation anomalies (mm day$^{-1}$) onto the first and second expansion coefficient time series of the right singular vectors of the SVD analysis. Percent covariance explained by each mode is given in the title of each plot. (facing page) The eigenvalue spectrum for the first five covariance modes from each precipitation dataset: CMAP (solid black), ICTP (dashed black), and ERA-40 (solid gray).

Ocean are in phase in terms of SST anomalies, similar to that shown in Fig. 6; however, for the 1950–78 period, they are out of phase. In the precipitation domain, RSV-2 (Fig. 7) shows a more meridional tripole pattern, with positive anomalies along the equator flanked by negative anomalies to the north and south, compared to that

from 1979 to 2000 (Fig. 6). Furthermore, the magnitude of the precipitation anomalies in Fig. 7 is lower than in Fig. 6. These lower amplitudes suggest a weaker linear relationship between SSTs and precipitation for the 1950–2000 period versus the 1979–2000 period, which could increase reconstruction errors. Overall, the
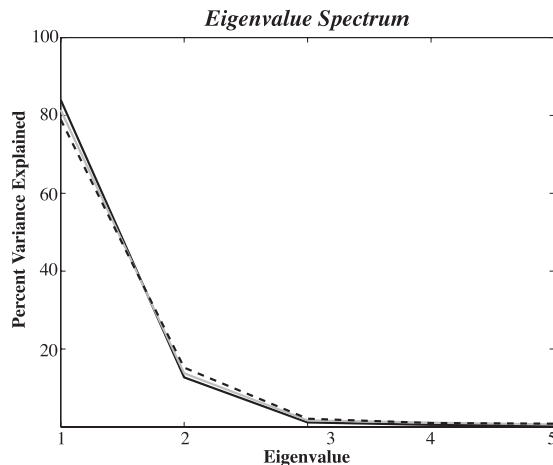
**Eigenvalue Spectrum**

Fig. 6. (*Continued*)

differences in the second covariability mode between the 1979–2000 statistics and the 1950–78 statistics suggest high sensitivity of our precipitation–SST relationship to the analysis period chosen.

Based on these findings, we conduct two new reconstructions whereby the mapping matrix in the multiregression method (**E**) consists of the covariability of tropical precipitation from the ICTP model run and tropical SST anomalies from NOAA ER SSTs from 1950 to 2000, but SST reconstructions are evaluated for 1) 1950–2000, using model precipitation for the input precipitation vector (**x**), and 2) 1979–2000, using CMAP precipitation data for **x**. The first analysis tests how well the results presented in section 3b hold for the longer time period. The latter case tests the possibility of using model-derived statistics from long integrations for climate pattern templates in lieu of data from the relatively shorter observational records of precipitation.

The first case (SST reconstructions for 1950–2000 using model precipitation over the whole period, Fig. 8) yields poorer performance for the reconstructions than the 1979–2000 case (see Fig. 4). Rms errors nearly double in the cold tongue region (0.1°–0.2°C), but larger changes are seen in the skill of the reconstruction (Fig. 8b). High reconstructive skill is now restricted to the central and eastern tropical Pacific Ocean, and those skill values are about 25% lower than their counterparts in Fig. 4. Larger skill degradation is seen in the Indian Ocean and west Pacific warm pool region. The estimated skill field (Fig. 8c) reflects these changes in skill for the larger sample, though amplitudes are overestimated particularly in the west Pacific warm pool region. Finally, the spatial correlation coefficients (Fig. 8d) have higher temporal variance than Fig. 5b (gray curve) displays, but the coefficients are still all positive and the mean correlation co-

efficient for the 51-yr period (0.66) is above the 95% significance level.

When considering the case of model-derived statistics from 1950 to 2000 with observational precipitation from 1979 to 2000 (Fig. 9), the tropical SST reconstructions are even more degraded in skill than the reconstructions that use only instrumental data from 1979 to 2000. Note that the estimated skill levels (Fig. 9c) are identical to those in Fig. 8c since the same joint statistics are used in the multiregression model. The rms errors (Fig. 9a) approach 0.5°C in the far eastern tropical Pacific, and the mean skill of the reconstructions (Fig. 9b) displays only moderate skill (~0.5) throughout the eastern part of the tropical Pacific Ocean. In fact, the demonstrated skill in this case is almost similar (and even less) than the skill shown using the EOF method for the eastern tropical Pacific (cf. Fig. 3, top row, middle column with Fig. 9b). Skill decreases by approximately 40% in the tropical Pacific Ocean between Fig. 4 (top row, middle column) and Fig. 9b. Furthermore, little if any skill is demonstrated in the west Pacific warm pool region or the Indian Ocean. Finally, the mean spatial correlation coefficients (Fig. 9d) are no longer uniformly positive, and the mean correlation coefficient is statistically insignificant ($r = 0.55$). Only 10 of the 22 years (~45%) have significant spatial correlations between the reconstructed and observed SST anomalies, compared to 86% (19 of the 22 years) in Fig. 5a (gray curve).

Thus, when the multiregression method is repeated using joint statistics of precipitation and SSTs from 1950 to 2000, the skill of the SST reconstructions decreases versus those performed using 1979–2000 statistics. Our observational analysis points to changes in LSV-2 and RSV-2 as the cause of the diminished skill. This change in the second leading mode of covariability likely reflects changes in the ENSO phenomenon. Implications of the change in this covariability mode may extend beyond tropical SST reconstructions to extratropical climate variability, owing to the far-reaching effects of tropical Indo-Pacific climate variability (e.g., Hoskins and Karoly 1981; Barsugli and Sardeshmukh 2002; Hoerling and Kumar 2002; Alexander et al. 2002).

## 5. Using the multiregression method with a realistic paleoprecipitation pseudoproxy network

The previous analyses examined the sensitivity of tropical SST reconstructions to both the method employed and the degree of stationarity in the climate statistics. In this section, we reconstruct tropical SST anomalies by applying the multiregression method to precipitation anomalies from locations corresponding to the pseudoproxy network defined in Table 1. We also
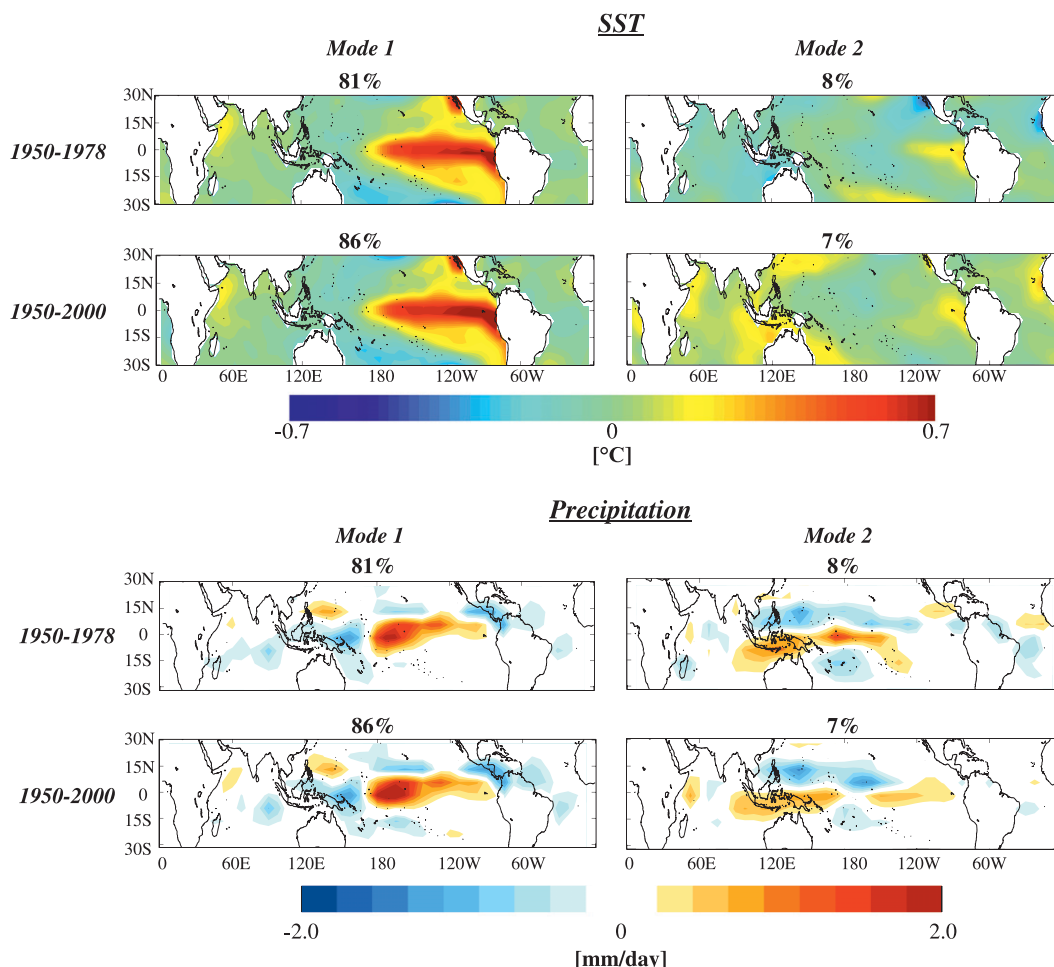
FIG. 7. The two leading modes of covariance between tropical SST and ICTP model precipitation anomalies (30°S–30°N) for two different periods: 1950–78 and 1950–2000. (top) Regression of annual-mean SST anomalies (°C) onto the first two expansion coefficient time series from the left singular vectors of the SVD analysis. (bottom) Regression of ICTP precipitation anomalies onto the first two expansion coefficient time series from the right singular vectors of the SVD analysis. Percent covariance explained by each mode is given in the title of each plot.

consider the effects of errors in the proxy data on the resulting tropical SST reconstructions. For brevity, only results using CMAP data are shown; however, findings are similar if precipitation fields from the model control run or ERA-40 are used (not shown).

### a.  SST reconstructions with the pseudoproxy network

Figure 10 displays the error statistics for tropical SST anomaly reconstructions for the period 1979–2000 using multiregression and the precipitation proxy network in Table 1. The rms error (Fig. 10a) and mean skill fields (Fig. 10b) illustrate that the network is able to capture SST anomalies in the central and eastern tropical Pacific Ocean when compared to the full-field reconstructions (Fig. 4, top row). Higher rms errors and consequently less skill exist for SST anomalies closer to the South

American coast, despite having several precipitation proxies nearby. Reconstructive skill in the Indian Ocean, however, is now lost with this pseudoproxy network (Fig. 10b). The mean skill matches well with the analytical estimate (Fig. 10c), while the spatial correlation coefficients are all positive with a statistically significant mean correlation of 0.67 (compared to 0.73 in Fig. 5a, gray curve). Overall, our specific pseudoproxy network captures almost 80% of the skill displayed using the full CMAP tropical precipitation field in the tropical Pacific, but only half of the skill in the Indian Ocean Basin.

### b.  Error propagation analysis

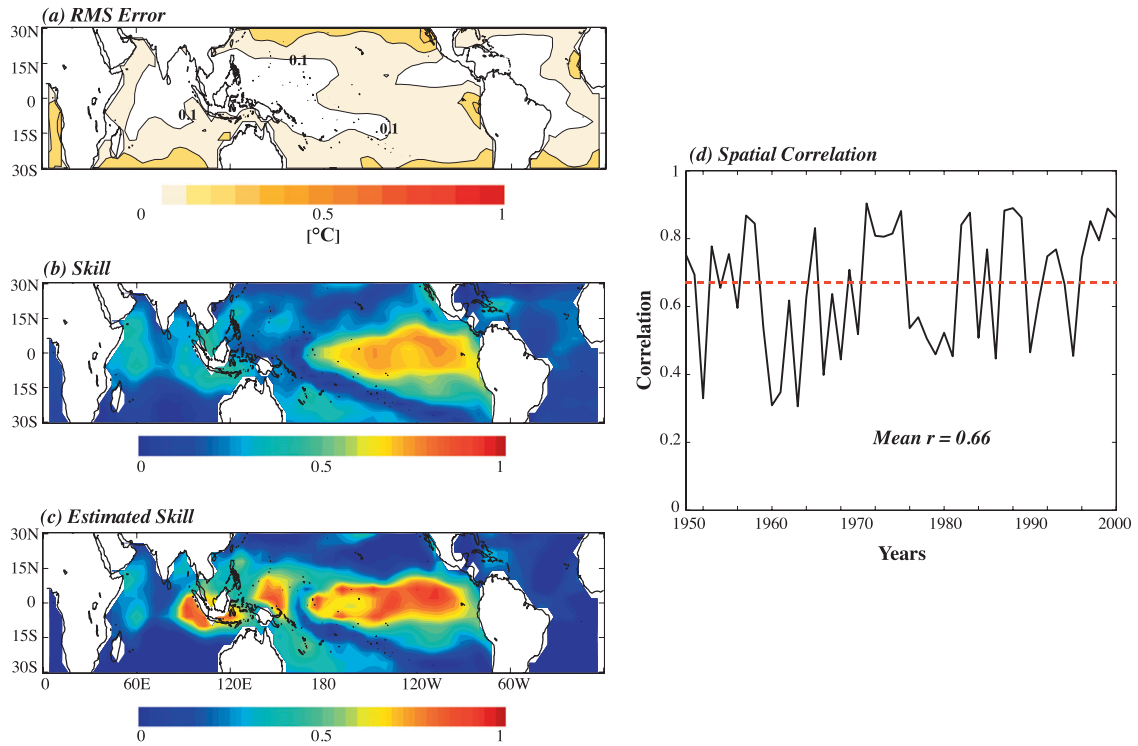The decrease in reconstructive skill using the pseudoproxy network suggests that the selected proxy

FIG. 8. Evaluation of the multiregression method using NOAA ER SSTs and ICTP model precipitation fields from 1950–2000: (a) rms error (°C). Contour interval 0.1°C; the 0.1°C contour is labeled for reference. (b) Reconstructive skill (dimensionless). (c) Estimated reconstructive skill (dimensionless). (d) Spatial correlation between the reconstructed and observed SST anomalies from 1950 to 2000. Red dashed line represents the 95% significance levels ($r = 0.64$). The mean correlation coefficient for the 51 years is also given.

network is missing key regions that are important for tropical SST reconstructions. In this section, we explore the importance of the spatial distribution of the proxy network sites and the potential errors associated with the precipitation proxy data.

To investigate the impact of errors in the pseudo-proxy network on SST anomaly reconstructions, we make use of (8) and include a term on the right-hand side, $\mathbf{n}_p$, representing errors associated with the precipitation records contained in $\mathbf{x}$. With this additional error term, the estimate of SST anomalies now changes by some quantity, denoted $\mathbf{n}_{SST}$, changing (8) to $\hat{\mathbf{y}} + \mathbf{n}_{SST} = \mathbf{E}(\mathbf{x} + \mathbf{n}_p)$, where $\mathbf{E}$ is given by (7). From here, we directly find that

$$\mathbf{n}_{SST} = \mathbf{E}\mathbf{n}_p. \qquad (13)$$

Equation (13) indicates that errors in precipitation are linearly related to errors in SST reconstructions via $\mathbf{E}$. For this analysis, precipitation errors are defined as

$$\mathbf{n}_p = \sqrt{\frac{\text{var}(\mathbf{x})}{\text{SNR}}},$$

where SNR is the signal-to-noise ratio. Furthermore, we test the impact of the spatial distribution of these errors by assigning nonzero $\mathbf{n}_p$ at all proxy sites and then assigning nonzero $\mathbf{n}_p$ only to specific sites in the proxy network.

Figure 11 illustrates the results of the error propagation analysis as a function of the SNR and the spatial location of errors. The absolute errors in SST anomalies range from 0° to 0.5°C, which is the same order of magnitude as the standard deviation in tropical Pacific SSTs (Fig. 2b), making these errors significant for climate reconstructions. As expected, decreasing the SNR (i.e., increasing $\mathbf{n}_p$) creates larger absolute errors in the reconstructions. SST anomalies in the west Pacific warm pool are the exception—there, SST errors remain near zero for both cases because rms errors are low already (Fig. 10a). Comparing rows in Fig. 11 (i.e., examining the dependence of $\mathbf{n}_{SST}$ on the spatial distribution of $\mathbf{n}_p$), errors in easternmost tropical Pacific SSTs are larger when $\mathbf{n}_p$ is nonzero for *Eastern* Hemisphere proxy sites versus when $\mathbf{n}_p$ is nonzero in the *Western* Hemisphere (cf. the second and third rows of Fig. 11). These regions include the few proxy sites in and near the Indian Ocean
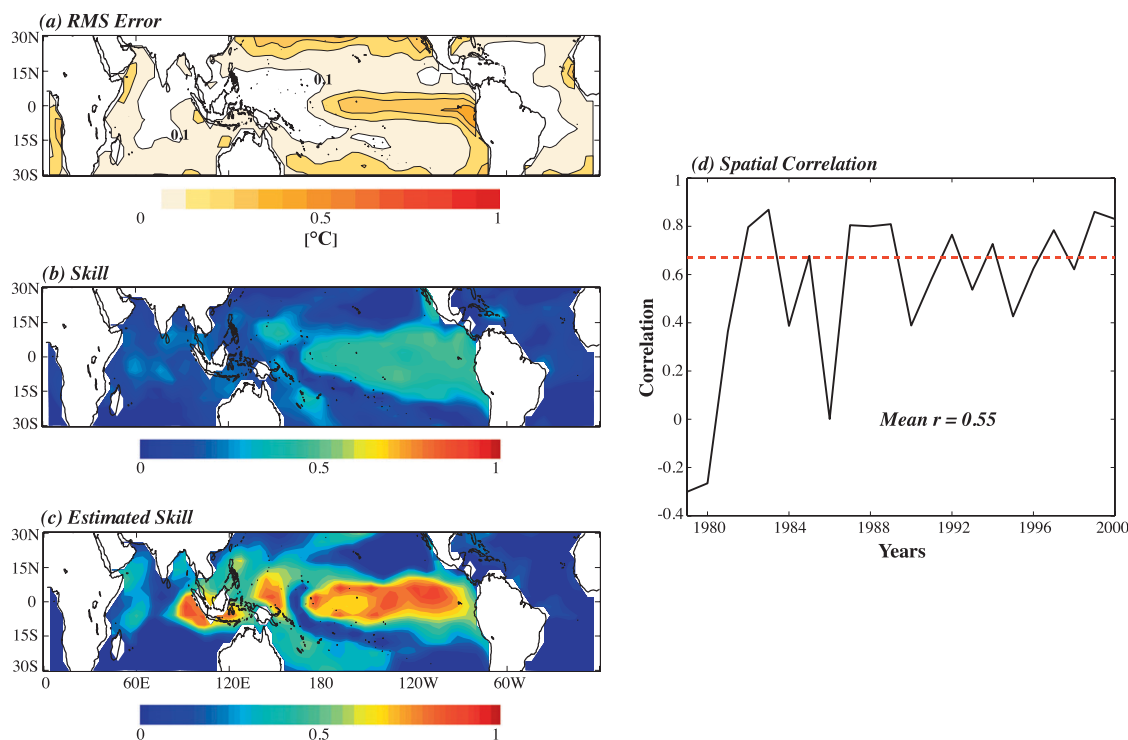
FIG. 9. As in Fig. 8 except evaluating SST anomaly reconstructions from 1979 to 2000 using SST–precipitation joint statistics from the ICTP model output for **E** and CMAP precipitation for **x** in the multiregression model.

as well as those near Australia and the poleward flank of the South Pacific convergence zone (SPCZ) (e.g., Streten 1973; Spencer 1993). Surprisingly, estimates of SST anomalies over the cold tongue region are less accurate when proxy sites in the Western Hemisphere have no error. This finding could be because of the greater number of ENSO-sensitive pseudoproxy sites in the Eastern Hemisphere. Another interesting possibility is that Eastern Hemisphere proxies capture key dynamical links between the Indian Ocean and the tropical Pacific Ocean, a topic garnering significant attention in tropical climate studies (Barnett 1984; Yu et al. 2002; Kug and Kang 2006).

Outside of the tropical Pacific cold tongue region, the regions that are most sensitive to errors in proxy precipitation anomalies lie in the northwest and southwest Pacific Ocean. In the Indian Ocean, $\mathbf{n}_{SST}$ is more dependent on the SNR than on the spatial distribution of $\mathbf{n}_p$ in the proxy network, though $\mathbf{n}_{SST}$ is small there anyway. Based on this analysis and our earlier evaluations of the reconstruction methods, assessing SST reconstructive skill in the Indian Ocean remains difficult, primarily because of the small variance in SSTs exhibited in this basin (Fig. 2b).

SNR values used in this study are one to two orders of magnitude higher than those used in other pseudoproxy studies (e.g., Mann and Rutherford 2002; Mann et al.

2007). Mann et al. (2007) relate their SNR choices to the average correlation of the proxy data from their network to a local climate signal (temperature) with the equation $r = \text{SNR}/(1 + \text{SNR}^2)^{1/2}$. Using the same equation for SNR = 10 (SNR = 2), the implied correlation of the proxy data from our multiproxy network with local precipitation anomalies is 0.99 (0.89). While we assumed a very large correlation for the proxies by choosing such SNR values in this analysis, SST errors in the cold tongue region are still significant (~1 standard deviation) when $\mathbf{n}_p$ is nonzero in Eastern Hemisphere records. For comparison, with SNR = 0.4 ($r = 0.37$), errors in the central tropical Pacific are ~1.0–1.2°C when $\mathbf{n}_p$ is nonzero in Eastern Hemisphere records (not shown). Therefore, although our SNR values are large compared to other studies, our study focuses on the spatial dependence of the SST reconstructive skill (i.e., how Indian Ocean proxies affect tropical Pacific SST reconstructions).

## 6. Discussion and conclusions

The results presented in this paper offer insight into the feasibility of using two popular methods that have been applied for SST anomaly reconstructions over the last millennium. This study uses tropical precipitation anomalies to directly estimate tropical SST anomalies.
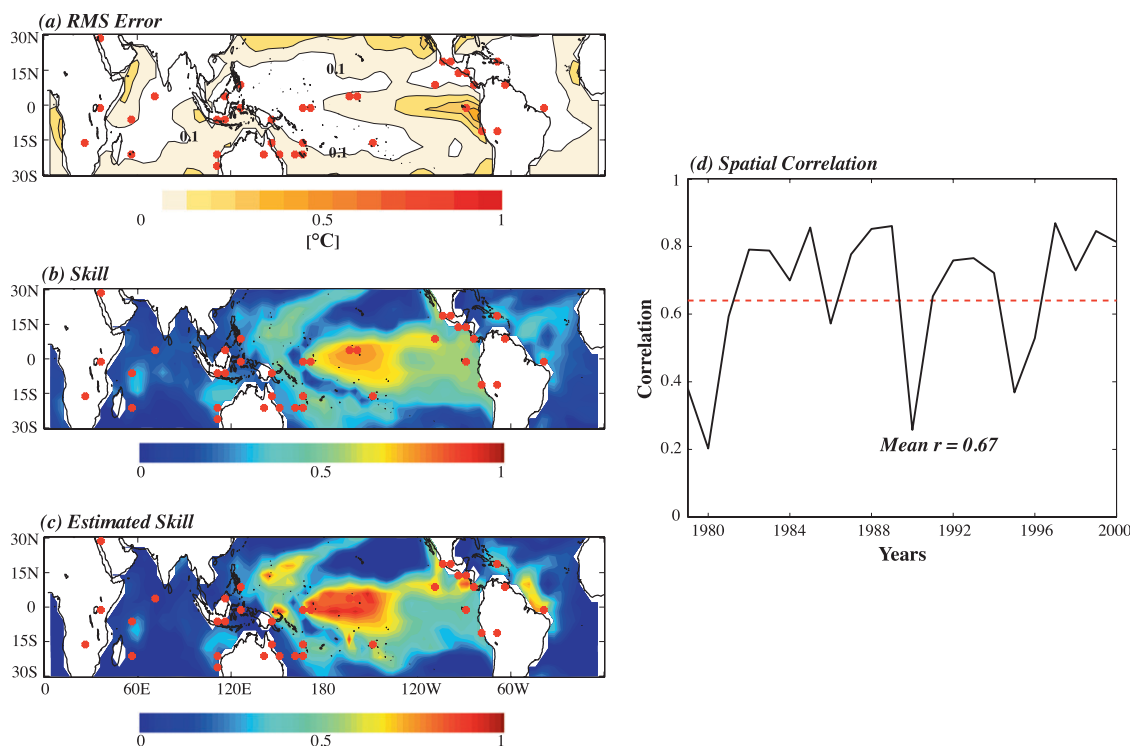
FIG. 10. Evaluation of the multiregression method for SST anomaly reconstructions from 1979 to 2000 using paleo-precipitation pseudoproxies from the network in Table 1. (a) Rms error (°C). Contour interval 0.1°C; the 0.1°C contour is labeled for reference. (b) Reconstructive skill (dimensionless). (c) Estimated reconstructive skill (dimensionless). (d) Spatial correlation between the reconstructed and observed SST anomalies from 1979 to 2000. Red dashed line represents the 95% significance level ($r = 0.64$). The mean correlation coefficient for the 22 yr is also given. Red dots in (a)–(c) represent the locations of the pseudoproxies.

Since many proxies used in reconstruction efforts do record past precipitation more directly than past SSTs, this approach outlines strategies for taking advantage of such paleoprecipitation records. Furthermore, as these strategies are based on dynamical links that exist between tropical precipitation and SST anomalies, they provide additional insights into the coupled ocean–atmosphere system. We have shown that much of the variance (>80%) of the observed SST anomalies can be reconstructed using the multiregression method, which significantly outperforms the EOF method in the tropical Pacific and Indian Oceans. The advantage of the multiregression method lies in the second mode of covariability between SSTs and precipitation, which explains nearly 15% of the covariability between the two variables. Identifying the dynamics that underlie this mode is therefore critical to accurate tropical SST reconstructions. Indeed, the presence of this mode of covariability in model-based or observational data should be a prerequisite for the pursuit of tropical Pacific SST reconstructions.

Moreover, transient changes in the SST–precipitation statistical relationship limit the skill of tropical SST re-

constructions. The degradation in reconstructive skill experienced between using 1979–2000 and 1950–2000 statistics clearly illustrates that reconstructions done using the multiregression method are sensitive to shifts in the climate system, such as that which occurred in 1976–77. This regime change is associated with changes in the evolution of individual ENSO events that altered the tropical SST–precipitation relationship. Developing reconstruction methods that account for different ENSO modes would therefore greatly improve Indo-Pacific SST reconstructions. First, though, the characteristics (and actual existence) of the $S$ and $T$ modes of ENSO should be further studied via ensembles and long integrations of a coupled GCM. These studies would also create a larger sample size for climate statistics that could be used in the multiregression method to obtain more robust results.

This study also provides some insight on the design of optimal networks of paleoprecipitation records for tropical SST reconstructions. The realistic paleoprecipitation proxy network chosen for this study preserves much of the reconstructive skill achieved when full-field tropical precipitation data are used. Decreased
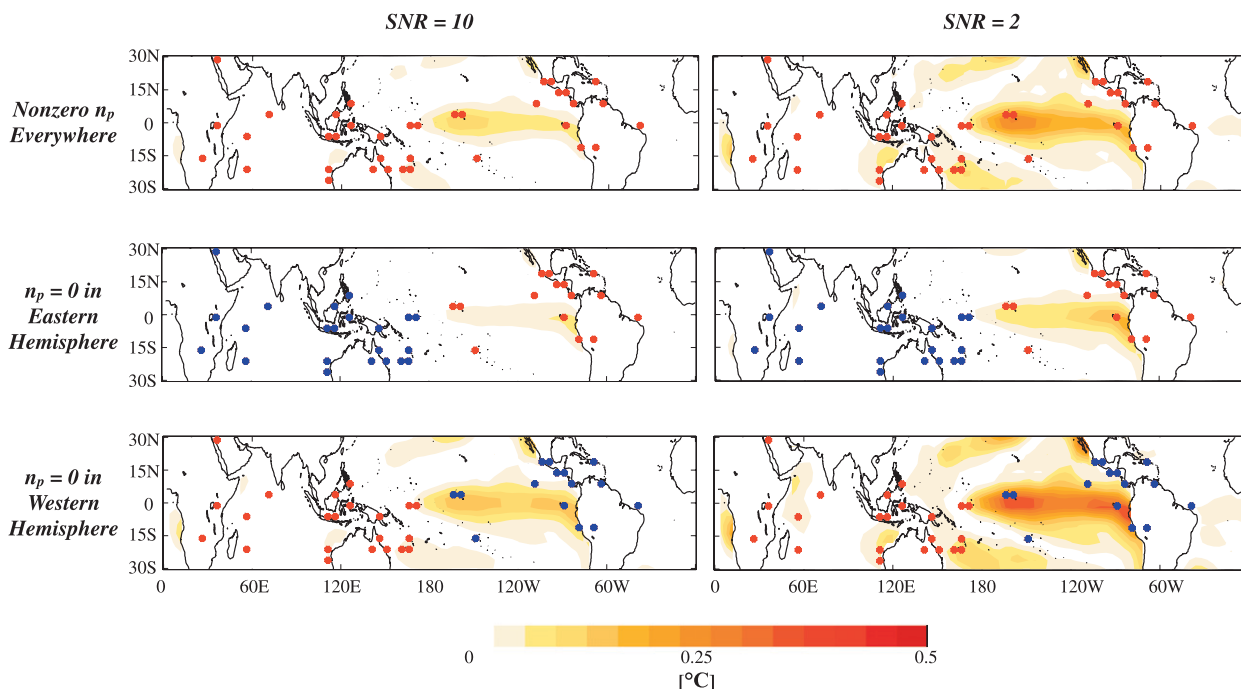
FIG. 11. The absolute error of the SST reconstructions (°C) using the multiregression method resulting from assumed errors ($\mathbf{n}_p$) in CMAP precipitation records in the pseudoproxy network. Red dots show the locations where nonzero $\mathbf{n}_p$ is applied to pseudoproxies, while blue dots indicate perfect pseudoproxies (i.e., $\mathbf{n}_p = 0$). Each case is also labeled on the left-hand side. Absolute errors also shown as a function of SNR: (left) SNR = 10; (right) SNR = 2.

proxy-based skill in the Indian Ocean may reflect the low number of proxies located in the Indian Ocean (Fig. 2a) and/or gaps in the network from remote locations where precipitation is sensitive to Indian Ocean SSTs. A similar explanation may apply to decreased reconstructive skill throughout the tropical Pacific Ocean when using the proxy network. Indeed, the error propagation analysis illustrates the importance of proxies in the Indian Ocean and SPCZ region for improved skill in tropical Indo-Pacific SST reconstructions (Fig. 11). Previous studies (e.g., Evans et al. 1998, 2002) corroborate these findings and highlight the importance of Indian Ocean proxy records for tropical Pacific SST reconstructions. Future modeling studies of coupled dynamics between the Indian and tropical Pacific Oceans would help to identify specific regions in the Indian Ocean for proxy generation. Precipitation sensitivity studies using adjoint models (e.g., $\mathbf{E}^T$ for the multiregression model, Wunsch 2006) could also prove valuable in designing an optimal paleoprecipitation network. The complication with this approach is the low variance in the Indian Ocean compared to the tropical Pacific Ocean, which makes it harder to identify SST-related precipitation changes.

This work illustrates the utility of performing climate field reconstructions to expand our current understanding of the climate system. By examining errors in both space and time, we identified several additional research questions related to tropical climate dynamics. Such reconstructions therefore offer a distinct advantage over reconstructions focused on a single index (e.g., Northern Hemisphere temperature or the Niño-3.4 index), which do not provide any dynamical insight.

REFERENCES

Alexander, M. A., I. Bladé, M. Newman, J. R. Lanzante, N.-C. Lau, and J. D. Scott, 2002: The atmospheric bridge: The influence of ENSO teleconnections on air–sea interaction over the global oceans. *J. Climate,* **15,** 2205–2231.

Barnett, T. P., 1984: Interaction of the monsoon and Pacific trade wind system at interannual time scales. *Mon. Wea. Rev.,* **112,** 2380–2387.

Barsugli, J. J., and P. D. Sardeshmukh, 2002: Global atmospheric sensitivity to tropical SST anomalies throughout the Indo-Pacific basin. *J. Climate,* **15,** 3427–3442.

Bell, G. D., M. S. Halpert, V. E. Kousky, M. E. Gelman, C. F. Ropelewski, A. V. Douglas, and R. C. Schnell, 1999: Climate assessment for 1998. *Bull. Amer. Meteor. Soc.,* **80,** S1–S48.

Biondi, F., 2001: A 400-year tree-ring chronology from the tropical treeline of North America. *Ambio,* **30,** 162–166.

Boiseau, M., M. Ghil, and A. Juillet-Leclerc, 1999: Climatic trends and interdecadal variability from south-central Pacific coral records. *Geophys. Res. Lett.,* **26,** 2881–2884.

Bracco, A., F. Kucharski, F. Molteni, W. Hazeleger, and C. Severijns, 2006: A recipe for simulating the interannual variability of the Asian summer monsoon and its relation with ENSO. *Climate Dyn.,* **28,** 441–460.

Bradley, R. S., M. Vuille, D. Hardy, and L. G. Thompson, 2003: Low latitude ice cores record Pacific sea surface temperatures. *Geophys. Res. Lett.,* **30,** 1174, doi:10.1029/2002GL016546.

Bretherton, C. S., C. Smith, and J. M. Wallace, 1992: An intercomparison of methods for finding coupled patterns in climate data. *J. Climate,* **5,** 541–560.

Charles, C. D., D. E. Hunter, and R. G. Fairbanks, 1997: Interaction between the ENSO and the Asian Monsoon in a coral record of tropical climate. *Science,* **277,** 925–928.

——, K. M. Cobb, M. D. Moore, and R. G. Fairbanks, 2003: Monsoon-tropical ocean interaction in a network of coral records spanning the 20th century. *Mar. Geol.,* **201,** 207–222.

Cobb, K. M., C. D. Charles, and D. E. Hunter, 2001: A central tropical Pacific coral demonstrates Pacific, Indian, and Atlantic decadal climate connections. *Geophys. Res. Lett.,* **28,** 2209–2212.

Cole, J. E., and R. G. Fairbanks, 1990: The Southern Oscillation recorded in the oxygen isotopes of corals from Tarawa Atoll. *Paleoceanography,* **5,** 669–683.

——, R. B. Dunbar, T. R. McClanahan, and N. Muthiga, 2000: Tropical Pacific forcing of decadal variability in the western Indian Ocean over the past two centuries. *Science,* **287,** 617–619.

Curtis, J. H., M. Brenner, D. A. Hodell, R. A. Balser, G. A. Islebe, and H. Hooghiemstra, 1998: A multi-proxy study of Holocene environmental change in the Maya lowlands of Peten, Guatemala. *J. Paleolimnol.,* **19,** 139–159.

Dai, A., and T. M. L. Wigley, 2000: Global patterns of ENSO-induced precipitation. *Geophys. Res. Lett.,* **27,** 1283–1286.

D'Arrigo, R. D., G. C. Jacoby, and P. J. Krusic, 1994: Progress in dendroclimatic studies in Indonesia. *Terr. Atmos. Oceanogr. Sci.,* **5,** 349–363.

——, E. R. Cook, R. J. Wilson, R. Allan, and M. E. Mann, 2005: On the variability of ENSO over the past six centuries. *Geophys. Res. Lett.,* **32,** L03711, doi:10.1029/2004GL022055.

Druffel, E. R. M., and S. Griffin, 1993: Large variations of surface ocean radiocarbon: Evidence of circulation changes in the southwestern Pacific. *J. Geophys. Res.,* **98,** 20 246–20 259.

Dunbar, R. B., G. M. Wellington, M. W. Colgan, and P. W. Glynn, 1994: Eastern Pacific sea surface temperature since 1600 A.D.: The $\delta^{18}$O record of climate variability in Galápagos corals. *Paleoceanography,* **9,** 291–315.

Evans, M. N., A. Kaplan, and M. A. Cane, 1998: Optimal sites for coral-based reconstruction of global sea surface temperature. *Paleoceanography,* **13,** 502–516.

——, R. G. Fairbanks, and J. L. Rubenstone, 1999: The thermal oceanographic signal of El Niño reconstructed from a Kiritimati Island coral. *J. Geophys. Res.,* **104,** 13 409–13 421.

——, A. Kaplan, and M. A. Cane, 2002: Pacific sea surface temperature field reconstruction from coral $\delta^{18}$O data using reduced space objective analysis. *Paleoceanography,* **17,** 1007, doi:10.1029/2000PA000590.

Federov, A. V., and S. G. Philander, 2000: Is El Niño changing? *Science,* **288,** 1997–2002.

——, and ——, 2001: A stability analysis of tropical ocean–atmosphere interactions: Bridging measurements and theory of El Niño. *J. Climate,* **14,** 3086–3101.

——, and ——, 2003: Is El Niño sporadic or cyclic? *Annu. Rev. Earth Planet. Sci.,* **31,** 579–594.

Guilderson, T. P., and D. P. Schrag, 1999: Reliability of coral isotope records from the western Pacific warm pool: A comparison using age-optimized records. *Paleoceanography,* **14,** 457–464.

Guilyardi, E., 2006: El Niño–mean state–seasonal cycle interactions in a multi-model ensemble. *Climate Dyn.,* **26,** 329–348.

Haug, G. H., K. A. Hughen, D. M. Sigman, L. C. Peterson, and U. Röhl, 2001: Southward migration of the Intertropical Convergence Zone through the Holocene. *Science,* **293,** 1304–1308.

Heiss, G. A., 1994: Coral reefs in the Red Sea: Growth, production and stable isotopes. GEOMAR Tech. Rep. 32, 141 pp.

Hendy, E. J., M. K. Gagan, C. A. Alibert, M. T. McCulloch, J. M. Lough, and P. J. Isdale, 2002: Abrupt decrease in tropical Pacific sea surface salinity at end of Little Ice Age. *Science,* **291,** 1511–1514.

Hoerling, M. P., and A. Kumar, 2002: Atmospheric response patterns associated with tropical forcing. *J. Climate,* **15,** 2184–2203.

Hoskins, B. J., and D. J. Karoly, 1981: The steady linear response of a spherical atmosphere to thermal and orographic forcing. *J. Atmos. Sci.,* **38,** 1179–1196.

Kucharski, F., F. Molteni, and J. H. Yoo, 2006: SST forcing of decadal Indian monsoon rainfall variability. *Geophys. Res. Lett.,* **33,** L03709, doi:10.1029/2005GL025371.

——, A. Bracco, J. H. Yoo, and F. Molteni, 2007: Low-frequency variability of the Indian monsoon–ENSO relation and the tropical Atlantic: The "weakening" of the 80s and 90s. *J. Climate,* **20,** 4255–4266.

Kug, J.-S., and I.-S. Kang, 2006: Interactive feedback between ENSO and the Indian Ocean. *J. Climate,* **19,** 1784–1801.

Kuhnert, H., J. Pätzold, B. Hatcher, K.-H. Wyrwoll, A. Eisenhauer, L. B. Collins, Z. R. Zhu, and G. Wefer, 1999: A 200-year coral stable oxygen isotope record from a high-latitude reef off Western Australia. *Coral Reefs,* **18,** 1–12.

——, ——, K.-H. Wyrwoll, and G. Wefer, 2000: Monitoring climate variability over the past 116 years in coral oxygen isotopes from Ningaloo Reef, Western Australia. *Int. J. Earth Sci.,* **88,** 725–732.

Kutzbach, J. E., 1967: Empirical eigenvectors of sea-level pressure, surface pressure and precipitation complexes over North America. *J. Appl. Meteor.,* **6,** 791–802.

Linsley, B. K., R. B. Dunbar, G. M. Wellington, and D. A. Mucciarone, 1994: A coral-based reconstruction of Intertropical Convergence Zone variability over Central America since 1707. *J. Geophys. Res.,* **99,** 9977–9994.

——, L. Ren, R. B. Dunbar, and S. S. Howe, 2000a: El Niño Southern Oscillation (ENSO) and decadal-scale climate variability at 10°N in the eastern Pacific from 1893 to 1994: A coral-based reconstruction from Clipperton Atoll. *Paleoceanography,* **15,** 322–335.

——, G. M. Wellington, and D. P. Schrag, 2000b: Decadal sea surface temperature variability in the subtropical South Pacific from 1726 to 1997 A.D. *Science,* **290,** 1145–1148.

Lorenz, E. N., 1956: Empirical orthogonal functions and statistical weather prediction. Sci. Rep. No. 1, Statistical Forecasting Project, MIT, 48 pp.

Mann, M. E., and S. Rutherford, 2002: Climate reconstruction using 'pseudoproxies.' *Geophys. Res. Lett.,* **29,** 1501, doi:10.1029/2001gl014554.

——, R. S. Bradley, and M. K. Hughes, 1998: Global-scale temperature patterns and climate forcing over the past six centuries. *Nature,* **392,** 779–787.

——, S. Rutherford, E. Wahl, and C. Ammann, 2005: Testing the fidelity of methods used in proxy-based reconstructions of past climate. *J. Climate,* **18,** 4097–4107.

——, ——, ——, and ——, 2007: Robustness of proxy-based climate field reconstruction methods. *J. Geophys. Res.,* **112,** D12109, doi:10.1029/2006JD008272.

Michaelson, J., 1989: Long-period fluctuations in El Niño amplitude and frequency reconstructed from tree rings. *Aspects of Climate Variability in the Pacific and Western Americas, Geophys. Monogr.,* Vol. 55, Amer. Geophys. Union, 69–74.

Molteni, F., 2003: Atmospheric simulations using a GCM with simplified physical parameterization. I: Model climatology and variability in multi-decadal experiments. *Climate Dyn.,* **20,** 175–191.

Moy, C. M., G. O. Seltzer, D. T. Rodbell, and D. M. Anderson, 2002: Variability of El Niño/Southern Oscillation activity at millennial timescales during the Holocene epoch. *Nature,* **420,** 162–165.

Neelin, J. D., 1991: The slow sea surface temperature mode and the fast-wave limit: Analytic theory for a tropical interannual oscillations and experiments in a hybrid coupled model. *J. Atmos. Sci.,* **48,** 584–606.

——, M. Latif, and F.-F. Jin, 1994: Dynamics of coupled ocean-atmosphere models: The tropical problem. *Annu. Rev. Fluid Mech.,* **26,** 617–659.

North, G. R., T. L. Bell, R. F. Cahalan, and F. J. Moeng, 1982: Sampling errors in the estimation of empirical orthogonal functions. *Mon. Wea. Rev.,* **110,** 699–706.

Obukhov, A. M., 1947: Statistically homogeneous fields on a sphere. *Usp. Mat. Nauk,* **2,** 196–198.

Partin, J. W., K. M. Cobb, J. F. Adkins, B. Clark, and D. P. Fernadez, 2007: Millennial-scale trends in west Pacific warm pool hydrology since the Last Glacial Maximum. *Nature,* **449,** 452–455.

Patzöld, J., 1984: Growth rhythms recorded in stable isotopes and density bands in the reef coral *Porites lobata* (Cebu, Philippines). *Coral Reefs,* **3,** 87–90.

Pfeiffer, M., O. Timm, W.-C. Dullo, and S. Podlech, 2004: Oceanic forcing of interannual and multidecadal climate variability in the southwestern Indian Ocean: Evidence from a 160 year coral isotopic record (La Réunion, 55°E, 21°S). *Paleoceanography,* **19,** PA4006, doi:10.1029/2003PA000964.

Quinn, T. M., T. J. Crowley, and F. W. Taylor, 1996: New stable isotope results from a 173-year coral record from Espiritu Santo, Vanuatu. *Geophys. Res. Lett.,* **23,** 3413–3416.

——, ——, F. W. Taylor, C. Henin, P. Joannot, and Y. Join, 1998: A multicentury stable isotope record from a New Caledonia coral: Interannual and decadal sea surface temperature variability in the southwest Pacific since 1657 A.D. *Paleoceanography,* **13,** 412–426.

Rasbury, M., and P. Aharon, 2006: ENSO-controlled rainfall variability records archived in tropical stalagmites from the mid-ocean island of Niue, South Pacific. *Geochem. Geophys. Geosyst.,* **7,** Q07010, doi:10.1029/2005GC001232.

Rasmusson, E. M., and T. H. Carpenter, 1982: Variations in tropical sea surface temperature and surface wind fields as-sociated with the Southern Oscillation/El Niño. *Mon. Wea. Rev.,* **110,** 354–384.

Rayner, N. A., D. E. Parker, E. B. Horton, C. K. Folland, L. V. Alexander, D. P. Rowell, E. C. Kent, and A. Kaplan, 2003: Global analyses of sea surface temperature, sea ice, and night marine air temperature since the late nineteenth century. *J. Geophys. Res.,* **108,** 4407, doi:10.1029/2002JD002670.

Rein, B., A. Lückge, and F. Sirocko, 2004: A major Holocene ENSO anomaly during the Medieval period. *Geophys. Res. Lett.,* **31,** L17211, doi:10.1029/2004GL020161.

Rodbell, D., G. O. Seltzer, D. M. Anderson, D. B. Enfield, M. B. Abbott, and J. H. Newman, 1999: A high-resolution 15000 year record of El Nino driven alluviation in southwestern Ecuador. *Science,* **283,** 516–520.

Shen, G. T., J. E. Cole, D. W. Lea, L. J. Linn, T. A. McConnaughey, and R. G. Fairbanks, 1992: Surface ocean variability at Galapagos from 1936–1982: Calibration of geochemical tracers in corals. *Paleoceanography,* **7,** 563–588.

Simmons, A. J., and J. K. Gibson, 2000: The ERA-40 Project Plan. ERA-40 Project Rep. Series No. 1, 62 pp.

Smith, T. M., and R. W. Reynolds, 2003: Extended reconstruction of global sea surface temperatures based on COADS data (1854–1997). *J. Climate,* **16,** 1495–1510.

Spencer, R. W., 1993: Global oceanic precipitation from the MSU during 1979–91 and comparisons to other climatologies. *J. Climate,* **6,** 1301–1326.

Stahle, D. W., and Coauthors, 1998: Experimental dendroclimatic reconstruction of the Southern Oscillation. *Bull. Amer. Meteor. Soc.,* **79,** 2137–2152.

——, P. T. Mushove, M. K. Cleaveland, F. Roig, and G. A. Haynes, 1999: Management implications of annual growth rings in *Pterocarpus angolensis* from Zimbabwe. *For. Ecol. Manage.,* **124,** 217–229.

Stott, L., K. Cannariato, R. Thunell, G. H. Haug, A. Koutavas, and S. Lund, 2004: Decline of surface temperature and salinity in the western tropical Pacific Ocean in the Holocene epoch. *Nature,* **431,** 56–59.

Street-Perrott, F. A., D. S. Marchand, N. Roberts, and S. P. Harisson, 1989: Global lake-level variations from 18,000 to 0 years ago: A paleoclimatic analysis. U.S. Department of Energy Tech. Rep. 46, 44 pp.

Streten, N. A., 1973: Some characteristics of satellite observed bands of persistent cloudiness over the Southern Hemisphere. *Mon. Wea. Rev.,* **101,** 486–494.

Therrell, M. D., D. W. Stahle, M. K. Cleaveland, and J. Villanueva-Diaz, 2002: Warm season tree growth and precipitation over Mexico. *J. Geophys. Res.,* **107,** 4205, doi:10.1029/2001JD000851.

Thompson, L. G., E. Mosley-Thompson, J. F. Bolzan, and B. R. Koci, 1985: A 1500 year record of tropical precipitation recorded in ice cores from the Quelccaya Ice Cap, Peru. *Science,* **229,** 971–973.

——, ——, M. E. Davis, P.-N. Lin, K. A. Henderson, J. Cole-Dai, J. F. Bolzan, and K.-B. Liu, 1995: Late glacial stage and Holocene tropical ice core records from Huascarán, Peru. *Science,* **269,** 46–50.

——, and Coauthors, 2002: Kilimanjaro ice core records: Evidence of Holocene climate change in tropical Africa. *Science,* **298,** 589–593.

Trenberth, K. E., and J. W. Hurrell, 1994: Decadal atmosphere-ocean variations in the Pacific. *Climate Dyn.,* **9,** 303–319.

Tudhope, A. W., and Coauthors, 2001: Variability in the El Niño Southern Oscillation through a glacial–interglacial cycle. *Science,* **291,** 1511–1517.

Urban, F. E., J. E. Cole, and J. T. Overpeck, 2000: Influence of mean climate change on climate variability from a 155-year tropical Pacific coral record. *Nature,* **407,** 989–993.

Wallace, J. M., E. M. Rasmusson, T. P. Mitchell, V. E. Kousky, E. S. Sarachik, and H. von Storch, 1998: On the structure and evolution of ENSO-related climate variability in the tropical Pacific: Lessons from TOGA. *J. Geophys. Res.,* **103,** 14 241–14 259.

Winter, A., T. Oba, H. Ishioroshi, T. Watanabe, and J. Christy, 2000: Tropical sea surface temperatures: Two-to-three degrees cooler than present during the Little Ice Age. *Geophys. Res. Lett.,* **27,** 3365–3368.

Wunsch, C., 2006: Basic machinery. *Discrete Inverse and State Estimation Problems with Geophysical Fluid Applications,* Cambridge University Press, 19–151.

Wyrtki, K., 1975: El Niño—The dynamic response of the equatorial Pacific Ocean to atmospheric forcing. *J. Phys. Oceanogr.,* **5,** 572–584.

Xie, P., and P. A. Arkin, 1997: Global precipitation: A 17-yearmonthly analysis based on gauge observations, satellite estimates, and numerical model outputs. *Bull. Amer. Meteor. Soc.,* **78,** 2539–2558.

Yu, J.-Y., C. R. Mechoso, J. C. McWilliams, and A. Arakawa, 2002: Impacts of the Indian Ocean on the ENSO cycle. *Geophys. Res. Lett.,* **29,** 1204, doi:10.1029/2001GL014098.

Zhang, Y., J. M. Wallace, and D. S. Battisti, 1997: ENSO-like interdecadal variability: 1900–93. *J. Climate,* **10,** 1004–1020.

Zinke, J., W.-C. Dullo, G. A. Heiss, and A. Eisenhauer, 2004: ENSO and Indian Ocean subtropical dipole variability is recorded in a coral record off southwest Madagascar for the period 1659 to 1995. *Earth Planet. Sci. Lett.,* **228,** 177–194.